

Parallel replica dynamics with a heterogeneous distribution of barriers: Application to *n*-hexadecane pyrolysis

Oyeon Kum,^{a)} Brad M. Dickson, and Steven J. Stuart^{b)}

Department of Chemistry, Clemson University, Clemson, South Carolina 29634

Blas P. Uberuaga and Arthur F. Voter

Theoretical Division, Los Alamos National Laboratory, Los Alamos, New Mexico 87545

(Received 16 October 2003; accepted 25 August 2004)

Parallel replica dynamics simulation methods appropriate for the simulation of chemical reactions in molecular systems with many conformational degrees of freedom have been developed and applied to study the microsecond-scale pyrolysis of *n*-hexadecane in the temperature range of 2100–2500 K. The algorithm uses a transition detection scheme that is based on molecular topology, rather than energetic basins. This algorithm allows efficient parallelization of small systems even when using more processors than particles (in contrast to more traditional parallelization algorithms), and even when there are frequent conformational transitions (in contrast to previous implementations of the parallel replica algorithm). The parallel efficiency for pyrolysis initiation reactions was over 90% on 61 processors for this 50-atom system. The parallel replica dynamics technique results in reaction probabilities that are statistically indistinguishable from those obtained from direct molecular dynamics, under conditions where both are feasible, but allows simulations at temperatures as much as 1000 K lower than direct molecular dynamics simulations. The rate of initiation displayed Arrhenius behavior over the entire temperature range, with an activation energy and frequency factor of $E_a = 79.7$ kcal/mol and $\log A/s^{-1} = 14.8$, respectively, in reasonable agreement with experiment and empirical kinetic models. Several interesting unimolecular reaction mechanisms were observed in simulations of the chain propagation reactions above 2000 K, which are not included in most coarse-grained kinetic models. More studies are needed in order to determine whether these mechanisms are experimentally relevant, or specific to the potential energy surface used. © 2004 American Institute of Physics. [DOI: 10.1063/1.1807823]

I. INTRODUCTION

A comprehensive understanding of hydrocarbon pyrolysis, both in terms of the primary initiation events and the subsequent radical propagation reactions, is of enormous importance for both basic and applied research. Specifically, knowledge of the kinetics of hydrocarbon pyrolysis is useful for understanding the cracking process by which the heavier petroleum residues are converted to lighter hydrocarbons with more commercial value.^{1–4} For example, extremely high-temperature, low-conversion pyrolysis conditions can be used to maximize the ethylene yield.⁵ There has thus been considerable experimental and theoretical interest in the thermal cracking of high-molecular-weight hydrocarbons such as *n*-hexadecane for many decades.^{2,3,6,7} The major difficulty in the experimental studies lies in the extremely wide range of initiation and propagation reactions occurring simultaneously; it is difficult to predict reaction conditions that lead to desired product branching ratios and length distributions, because of the enormous number of intermediates involved.

Computational models are frequently used to predict product distributions as a function of reaction time.^{8–14} These kinetic models typically assume a system of coupled

differential equations representing the complex network of reactions. This system of equations can be integrated in time, and can provide a wealth of information regarding the reaction conditions needed to maximize the desired product fractions. However, these models require *a priori* knowledge of the detailed reaction mechanisms, activation energies, and frequency factors, which are currently obtained primarily from experiments.^{1,8,11,12,15} Many important reactions are not easily studied experimentally, and consequently most kinetic models lack well-defined parameters. Electronic structure calculations can potentially provide useful information about both the energetic and kinetic parameters for the reactions of interest, and provide a possible supplement to experiment in this regard.^{16–20} However, *ab initio* calculations are most practical on small hydrocarbons, and begin to become prohibitively expensive for larger gas oil hydrocarbons such as hexadecane. Even for small hydrocarbons, very high-level calculations are required in order to obtain accurate kinetic parameters.^{16,19,20} In addition, the number of candidate reactions and transition states grows rapidly with molecular size, making it less likely that Arrhenius parameters for all of the candidate reactions can be predicted and evaluated directly. The reactions chosen for detailed study thus depend heavily on (human) chemical intuition, and have not been explored in a comprehensive way.

This gap can be addressed by using classical models, at

^{a)}Electronic mail: okum@clemson.edu

^{b)}Electronic mail: ss@clemson.edu

considerably less computational expense than with quantum mechanical models. This requires a potential energy function for hydrocarbons that is capable of modeling covalent bonding reactions empirically.^{21–23} Because of the reduced computational expense, the possibility exists for observing mechanisms and obtaining kinetic data directly from dynamic calculations, rather than indirectly from static calculations at fixed points on the potential energy surface. Although such dynamics calculations have been performed in the past,^{24,25} they have been limited by the short simulation time scales achievable. Decomposition times in the microsecond to second range^{5,8,18} at experimentally relevant pyrolysis temperatures of 800–1400 K are inaccessible by conventional (serial) molecular dynamics (MD) simulations. Consequently, previous simulations^{24,25} have been run at temperatures above 3000 K in order to observe pyrolysis in simulation times of less than 1 ns. While these simulations can provide useful insights, the conditions permit high-barrier reactions that would not be observed at the lower temperatures, and hamper the ability to extrapolate the data and mechanistic information to lower temperatures.

One approach that can be used to solve the time scale problem is to apply parallel replica dynamics (PRD) (Ref. 26) by running several concurrent simulations that each independently explore the phase space of a given potential energy basin. When any of these processors detects a transition to a new state, all processors are then put to work in that new state. This method has been applied successfully to extend simulation time scales for diffusion processes with relatively narrow distributions of barrier heights.^{26,27} The potential energy surfaces for large alkanes are qualitatively quite different, with small barriers separating conformational states and much larger barriers separating isomers and dissociation products. We exploit this gap in the energy barrier spectrum to gain parallel efficiency, allowing the PRD algorithm to detect a transition only when a bonding change occurs. Lumping the conformational substrates together in this way is similar to the assumption made by Pande^{28,29} in his application of parallel replica dynamics to the folding of small proteins. Our transition detection procedure and the conditions under which it is a rigorous application of PRD are discussed in Sec. II. The combination of an accurate model for covalent hydrocarbon reactivity²³ with the parallel replica dynamics algorithm²⁶ and a suitably chosen transition-detection algorithm³⁰ has resulted in a simulation technique that allows classical dynamics simulations of hydrocarbon reactivity at physically meaningful time scales. Simulations of $O(1 \mu\text{s})$ were achieved, enabling realistic simulations of pyrolysis at temperatures of as low as 2100 K. These temperatures are much lower than the 3000 K temperatures (nanoseconds time scales) previously achieved with direct dynamics. They are still higher than the ~ 1100 K temperatures (milliseconds time scales) of interest for industrial processes, and considerably higher than the ~ 450 – 600 K temperatures of geologic interest,^{4,11} but are beginning to approach the temperature range of interest for high-temperature thermal decomposition of organic waste. Even longer simulation times and lower temperatures can be ac-

cessed quite straightforwardly by using more parallel processors.

The primary purpose of this study is to describe the transition detection algorithm and demonstrate the validity of the resulting PRD algorithm. This is done here for the case of hydrocarbon pyrolysis, but can be applied more widely to other systems in which large-barrier rare events take place in the presence of frequent small-barrier transitions. A secondary objective is to demonstrate how this method can be used to explore the potential energy surface for hydrocarbon pyrolysis, generating candidate reactions with classical potentials in an unbiased way, for more detailed study with additional methods. The specific kinetic and mechanistic conclusions depend strongly on the quality of the potential model used, and are independent from the more general conclusions regarding the simulation method. We summarize the parallel replica dynamics algorithm in Sec. II, along with the reactive hydrocarbon potential used for the simulations. The reaction mechanisms, reaction rates, and Arrhenius parameters for the gas phase decomposition of *n*-hexadecane in the temperature range of 2100–2500 K are presented in Sec. III. Finally, our conclusions are given in Sec. IV.

II. COMPUTATIONAL MODEL

A. Parallel replica dynamics

Parallel replica dynamics is an algorithm for parallelizing rare-event simulations in the time domain, rather than the spatial domain. The details of the original PRD algorithm appear in Ref. 26. We discuss the method briefly in this paper with particular emphasis on the modifications in the algorithm necessary to apply it to systems with a mixture of both fast and slow processes, such as gas-phase alkanes, where barriers separating conformational states are much lower than those preventing covalent bond dissociation.

The theoretical basis of PRD is to initiate M independent replica trajectories in the same energy basin with different initial velocity distributions. If k_{tot} represents the total rate constant for escape through any of the available escape routes, then individual replicas will have escape times distributed as

$$p(t)dt = k_{\text{tot}}e^{-k_{\text{tot}}t}dt. \quad (1)$$

In Eq. (1), we have assumed first-order escape kinetics, a requirement for PRD. This exponential decay arises naturally in the rare-event limit where the energy basin is well sampled on times much shorter than the average escape time.

Because the M replica systems all have statistically equivalent escape time distributions, the overall rate constant for the *first* escape time is simply Mk_{tot} . The distribution of first escape times in the M -replica aggregate system is

$$p(t)dt = Mk_{\text{tot}}e^{-Mk_{\text{tot}}t}dt, \quad (2)$$

which can be rewritten as

$$p(t_{\text{sum}})dt_{\text{sum}} = k_{\text{tot}}e^{-k_{\text{tot}}t_{\text{sum}}}dt_{\text{sum}}, \quad (3)$$

where $t_{\text{sum}} = Mt$ is the total time accumulated on all of the replica systems. Thus the distribution of cumulative times for the first escape on M independent replica systems [Eq. (3)] is

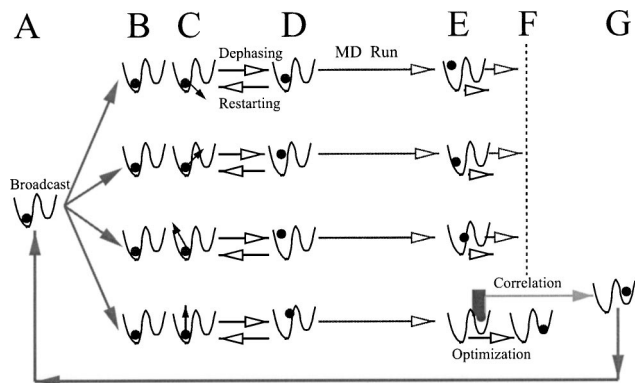


FIG. 1. Schematic diagram of the parallel replica dynamics algorithm.

identical to the distribution of escape times measured in a single simulation [Eq. (1)]. It is also easily demonstrated that the relative probabilities of sampling any particular escape path are unchanged.²⁶ Furthermore, if the replica systems are all reinitiated in the new basin after the first crossing and dephased—by using a stochastic thermostat, for example—then the transition time for the second and subsequent reactions can be similarly parallelized with different values of k_{tot} . This is important in that it allows for correct treatment of state-to-state dynamics in systems with complex reaction networks. The computational advantage for the M -replica system results from the very low communication overhead required to run the systems in parallel.

Figure 1 shows the schematic diagram of the parallel replica dynamics simulation algorithm. Computation starts with the master processor broadcasting initial configuration data (panel A) to all slave processors (panel B). Each processor generates independent initial momenta from a Maxwell-Boltzmann distribution at the desired temperature (panel C). To guarantee that the initial configuration information is also independent, each processor performs a subsequent “dephasing” run of length Δt_ϕ using thermostated dynamics (panel D). During the dephasing run, if any transition is detected, the processor returns to the original configuration and generates a new set of momenta, and runs the dephasing again until no transition is detected. When dephasing is complete, simulation time begins to be accumulated on each processor. The whole molecular dynamics simulation is divided into blocks of length Δt_b and a transition check is performed on each processor at the end of each simulation block (panel E). The block size was chosen to be $\Delta t_b = 1$ ps in the current study. Once any slave node detects a transition (panel F), it reports to the master node and the master node broadcasts the transition information to all nodes. When any slave node receives the message from the master node, it stops the calculation immediately and reports its simulation time to the master. The master node calculates the PRD transition time (t_{sum}) by summing all slave node simulation time since the end of the dephasing stage. Meanwhile, the processor detecting the transition runs for an additional correlation time Δt_c to allow for correlated recrossings or correlated multiple hops.³¹ The non-first-order dynamics during the correlation period is treated rigorously by not integrating it in parallel. The configuration at the end of the correlation time is then

broadcast to all other slaves (via the master) and the procedure is repeated, beginning with the dephasing period, in the new state. In this study, we chose a conservative value of Δt_c of 40 ps, which is longer than the 25 ps required for the dihedral angles to lose any correlation with their previous state, as measured with dihedral angle autocorrelation functions. This was the most slowly decaying of any single-angle autocorrelation function. There are slower, collective modes, such as those probed by the end-to-end distance or the radius of gyration, but we assume that the system is sufficiently decorrelated once it has made one or more conformational transitions (on average) about each C–C bond. The dephasing time Δt_ϕ was also chosen to be 40 ps in this study. Note that the careful treatment of dephasing and correlated transitions is crucial in PRD, and distinguishes this method from the more common practice of running independent simulations in parallel to enhance sampling and equilibrium averages. Parallelization of the dynamics (rather than increased sampling) allows determination of kinetic properties, such as reaction rates. This is only possible because the (rare-event) dynamics are first order, as in Eq. (1); this assumption must always be carefully monitored.

Because parallel communication is only necessary at the end of the coarse simulation blocks (rather than once or more per time step, as in traditional spatial approaches to parallelism), the PRD algorithm has low communication overhead, and a comparatively high parallel efficiency. Indeed, the initiation reactions discussed in the following section achieved parallel efficiencies of over 90% for $M = 60$ replicas on 61 processors. The overall efficiencies for the subsequent transitions were somewhat lower because the radical propagation reactions (with lower activation energies than the initiation reactions) frequently reacted during the 40 ps dephasing time and required multiple dephasing periods. In order to improve the overall efficiency, one could adjust the block times Δt_b after initiation to match the subsequent radical reaction times. This requires at least an approximate knowledge of the rate of reaction for each new state that is visited, however. In this study, we used the same block times for the entire duration of each PRD simulation.

Defining state-to-state transitions is a key component of PRD, and the appropriate method of transition detection depends on the system. In the previous metal surface studies, an energy minimization was performed at the end of each simulation block, and the resulting optimized configuration was compared to the optimized configuration determined when that state was initially entered.²⁷ If these configurations did not match, a transition was declared. This corresponds to defining each potential energy basin as a unique state. In the present study, we use a different approach, based instead on topological basins.

A hydrocarbon system is characterized by a mixture of low barriers separating a large number of conformational states and high barriers for reactions that change the bond connectivity. In studying pyrolysis, our interest lies in these high-barrier events. The low-barrier events are important to us only in the sense that we wish to allow their dynamical evolution to proceed accurately enough so that the high-barrier events occur when they should. In a formally com-

plete implementation of PRD, every passage between energy basins, including the low-barrier conformational changes, would be declared as a transition. These low-barrier transitions are so rapid, though (occurring every few picoseconds) that the dephasing and correlation overhead in PRD would cause the parallel efficiency to suffer if more than just a few processors were employed. Indeed, at elevated temperatures the dynamics among configurational states may not be first order, since the barrier heights are not small compared to kT (although PRD could always be applied rigorously at sufficiently low temperatures). However, we can exploit the gap between the conformational barriers (<10 kcal/mol) and the typical bond-breaking barriers (>20 kcal/mol for radicals, >80 kcal/mol for saturated hydrocarbons) to overcome this problem. We base the transition detection procedure on the bond connectivity, so that conformational transitions (which do not change the connectivity) are ignored. This effectively lumps all conformations with a given bond connectivity into a single "superstate." Each superstate thus corresponds to a unique isomer (or set of isomers of product molecules). The key requirement is that the transition rates among the conformational "microstates" in a given superstate are substantially faster than the rate of escape to the next superstate, so that the probability of escaping to a superstate is independent of which microstate the system starts in. If this assumption holds, then the first-passage time probability distribution function for the nonconformational transitions, $p(t)$, will be an exponential, as required by Eq. (1), and the PRD evolution among superstates will be dynamically valid. If there is not a large gap between the microstate transition rates and the superstate transition rates, then $p(t)$ will no longer be exponential and ignoring transitions in this way will lead to errors in the dynamics. We demonstrate in the following section that $p(t)$ is indeed an exponential to good accuracy for the hexadecane system at $T=2900$ K. Because the ratio of rate constants increases exponentially with decreasing temperature in this system, this superstate approximation becomes even better as the temperature is lowered.

It is interesting to note that there are $O(10^5)$ symmetrically distinct conformational states for the n -hexadecane superstate. While only a small fraction of these microstates are visited before escape to another superstate, the criterion for exponential behavior of $p(t)$ appears to be met nonetheless (see Fig. 2). The important condition is that the escape time be independent of the starting microstate, not that all microstates be visited. These two conditions are quite different in a system of high dimensionality. In order to fully sample the possible escape paths from the superstate, so that the probability of choosing a given superstate escape path is independent of the initial microstate (uncorrelated escapes), the trajectory must traverse the "width" of the system in configuration space many times. In a one-dimensional superstate, in which a chain of microstates is terminated with a high barrier at each end, the trajectory will necessarily visit each microstate many times if it visits each end of the chain many times. In contrast, in many dimensions, the system passes through only a small fraction of the microstates as it goes from one "end" to another along any one dimension. Depending on the nature of the system, a number of these

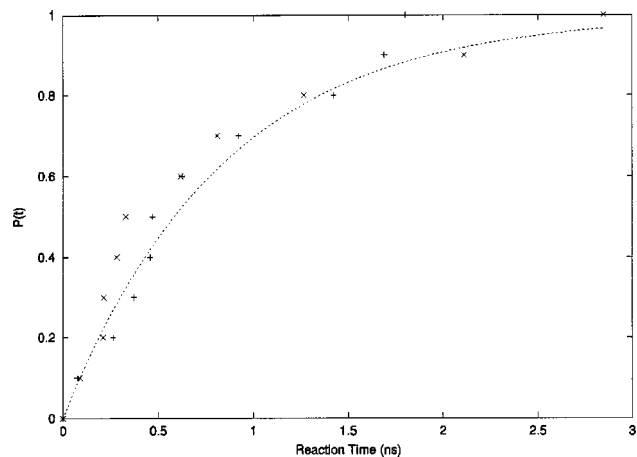


FIG. 2. Observed probability distribution $P(t)$ that a chain has undergone a reaction at time t for direct MD simulation (\times) and PRD simulation ($+$) at 2900 K. For a first-order process, these data would be described by $P(t) = 1 - e^{-kt}$. Both curves are well described by this distribution with $k = 1.19 \times 10^9 \text{ s}^{-1}$ (dashed line).

passes may be sufficient to sample the superstate escape paths fully enough to obtain uncorrelated escape from the superstate, even though many of the microstates may never be visited. We believe alkane molecules fall in this category because the covalent bonding reaction barriers depend on local conformational information (which is well sampled on short times) but do not appear to depend strongly on global conformation. The reaction coordinates for the high-barrier covalent bonding reactions are almost identical with the bond coordinate for the bond undergoing a chemical change, with almost no contribution from the dihedral angle coordinates that lead to conformational changes between microstates. In other words, there is no unique conformation from which bond dissociation must take place, and every conformation is one of the end states. Also, complex transition states [such as (1,5) hydrogen transfer via six-membered ring transition states] should cause no problem as long as representative local configurations (the six-membered ring conformation) are sampled on times shorter than the superstate escape time.

During the PRD simulations, a transition is declared whenever there is a change in the bond connectivity matrix \mathbf{A} , where $A_{ij} = 1$ or 0 based on whether there is, or is not, a bond between atoms i and j . In practice, this information is evaluated using the Verlet neighbor lists, and the definition of a covalent bond is an atom pair with a separation less than the covalent bonding cutoff r_{ij}^{max} in the adaptive intermolecular reactive empirical bond order (AIREBO) potential²³ used for the simulations. This is a natural way of identifying transitions between isomers and into different chemical species, while ignoring conformational transitions. In principle, such an approach does not require energy minimization at the end of each block, if covalent bonding can be reliably determined from nonminimized states. However, close-contact, nonreactive intramolecular collisions are common at high temperatures and cannot easily be distinguished from nascent bonds without optimization; we performed a full energy minimiza-

tion using steepest descent at the end of each block in this study.

By failing to detect (and rethermalize in) each conformational microstate, these simulations have lost the ability to correctly describe the diffusion or dynamics between the conformational states; diffusion among microstates is not accelerated in the same manner as transitions between superstates. As a consequence, the PRD time is not a deterministically correct time for any particular single trajectory. Instead, the PRD time must be interpreted as a statistically unbiased estimate of the reaction time at the moment of superstate transition.

This approach of aggregating energy basins (microstates) into larger groups (superstates) is related to the approach used by Pande.^{28,29} That work uses signatures in the energy variance to indicate when transitions have been made between large free energy basins along the protein folding pathway.³² Our system is considerably simpler, both in that the reactions of interest are easily identifiable once they have occurred and transition detection can be performed quantitatively.

We note that the separation in energy scales between chemical reactions and conformational transitions is not perfect. Although the activation energy for homolytic bond dissociation in saturated hydrocarbons is quite large (80–100 kcal/mol), the reverse reaction, radical combination, is nearly barrierless. This might be expected to introduce inefficiencies in the PRD algorithm, if fast recombinations require that much of the simulation time be spent in single-processor integration of the correlation time Δt_c . However, for gas-phase pyrolysis this is not a problem: the rate of the radical combination reactions is small, despite the low barrier. Kinetically, the frequency factor for the bimolecular combination reaction is much smaller than that of the unimolecular dissociation. The large loss of entropy in the combination reaction results in a significant free energy barrier to recombination, even though the energetic barrier is small. From a microscopic simulation point of view, products which dissociate with a nonzero velocity in an infinite simulation volume (no periodic boundary conditions) are vanishingly likely to reencounter one another. No such recombinations were observed to occur in this study. In higher density systems, such as liquid-phase pyrolysis, the presence of low-barrier radical reactions may indeed be a more serious problem.

B. AIREBO potential

We chose the AIREBO potential to describe hydrocarbon interactions in the pyrolysis simulations. This potential is described in detail elsewhere,²³ and we summarize it only briefly in this paper. This potential is one of a series of successful bond-order potentials for covalently bonded materials that originated with Tersoff's many-body potentials for silicon, carbon, and other semiconductors,³³ and continued with Brenner's parametrization for hydrocarbons.^{21,22} In these models, the covalent bonding interaction V_{ij} between two atoms i and j comprises contributions from a repulsive potential V_{ij}^R and an attractive potential V_{ij}^A both of which are pair potentials:

$$V_{ij}^{\text{REBO}}(r_{ij}) = V_{ij}^R(r_{ij}) + b_{ij}V_{ij}^A(r_{ij}). \quad (4)$$

The relative contribution of each term is modulated by the presence of the so-called "bond order" term b_{ij} . This term is responsible for the modification of bond strength and equilibrium bonding distance based on changes in the local bonding environment, and is responsible for the many-body nature of the potential (i.e., the bond-order term b_{ij} depends on the positions of atoms other than i and j). This class of models has been widely used for modeling chemical reactions in covalently bonded carbon and hydrocarbon systems. The Tersoff and Brenner (REBO) potentials differ primarily in the functional form chosen for the bond order b_{ij} .^{21,22,31}

While the AIREBO potential was primarily developed for condensed-phase systems, we chose it for the current studies of gas-phase hexadecane pyrolysis because it includes the ability to model torsional potentials about σ bonds, as well as including exchange repulsion and dispersion interactions.²³ The torsional interactions are crucial in describing the relative population of different conformers of hexadecane, and the van der Waals interactions are relevant to the distribution between extended and coiled molecular states. The conformational degrees of freedom may well be important in determining the mechanism and kinetics of the pyrolysis process, an effect that is not considered in nonatomistic kinetic models. The AIREBO potential describes the covalent bonding interactions largely as in Brenner's REBO potential.²² In addition, there are terms in the potential to account for torsional energies of single-bond rotations, as well as the nonbonded van der Waals interactions,

$$V_{ij}^{\text{AIREBO}} = V_{ij}^{\text{REBO}} + V_{ij}^{\text{tors}} + V_{ij}^{\text{vdW}}, \quad (5)$$

where V_{ij}^{REBO} is Brenner's REBO potential. The torsional energy is not modeled via the familiar truncated Fourier series, which imposes a predefined symmetry upon each rotatable bond, but is instead modeled as a pairwise interaction between (1,4) atoms,

$$V_{ij}^{\text{tors}}(\omega) = \epsilon \left[\frac{256}{405} \cos^{10}(\omega/2) - \frac{1}{10} \right], \quad (6)$$

where ω is the dihedral angle and ϵ characterizes the strength of the interaction. The advantage of this formulation of the torsional energy is that the symmetry of the dihedral angle potential is dictated entirely by the symmetry of the molecule, and can change as reactions occur. The van der Waals interaction is modeled using the standard Lennard-Jones (LJ) 12-6 potential, modified by several environment-dependent switching functions,

$$V_{ij}^{\text{vdW}} = \{S(r_{ij})[S'(b_{ij}^*) - 1] + 1\} C_{ij} V_{ij}^{\text{LJ}}, \quad (7)$$

$$V_{ij}^{\text{LJ}} = 4\epsilon \left[\left(\frac{\sigma_{ij}}{r_{ij}} \right)^{12} - \left(\frac{\sigma_{ij}}{r_{ij}} \right)^6 \right]. \quad (8)$$

The C_{ij} switching function is used to screen the LJ interactions between atoms that are connected by three or fewer covalent bonds; the $S'(b_{ij}^*)$ switching function is used to adaptively screen the repulsive LJ interactions, reducing them for atom pairs that are not bonded, but which will have large bond orders upon closer approach; and the $S(r_{ij})$ switching function is used to ensure that the long-range dis-

TABLE I. Initiation mode and reaction time (in nanoseconds) for ten independent starting configurations and five temperatures. (CCD=C–C dissociation; CHD=C–H dissociation.)

Temperature (K)	1	2	3	4	5	6	7	8	9	10
2500	CCD (11.63)	CHD (12.40)	CHD ^a (8.74)	CHD ^a (10.68)	CHD (6.95)	CHD (12.76)	CHD ^a (22.74)	CHD (4.32)	CHD (21.35)	CHD ^a (11.41)
2400	CHD (25.59)	CHD (12.99)	CHD (58.86)	CHD (1.26)	CHD (4.21)	CCD (7.30)	CCD (77.87)	CHD (42.82)	CHD ^a (12.64)	CHD (12.90)
2300	CHD (70.38)	CHD (155.32)	CHD (16.79)	CHD ^a (9.04)	CHD (0.04)	CHD ^a (1.54)	CHD ^a (36.17)	CHD (93.79)	CCD (179.17)	CHD (9.85)
2200	CHD (130.66)	CHD (40.79)	CHD ^a (39.69)	CHD (98.98)	CHD (21.76)	CCD (476.55)	CHD ^a (147.97)	CHD (19.56)	CHD (88.65)	CCD (319.42)
2100	CCD (74.01)	CHD (191.17)	CHD (37.19)	CCD (183.94)	CCD (236.94)	CHD (19.14)	CHD (22.59)	CHD (104.03)	CHD (783.41)	CHD (789.76)

^aPrimary CHD.

persion interactions are always present. Additional details about the AIREBO potential are available in Ref. 23.

III. RESULTS AND DISCUSSIONS

A. Validation

As discussed in the preceding section, the assumption of first-order kinetics [Eq. (1)] requires that the state (in this case the superstate) be sufficiently well sampled (or traversed) on time scales shorter than the average escape time. The PRD algorithm will fail if the events being sampled are not rare events, and the escape time distribution is not first order. In order to validate the chosen values for the dephasing time, correlation time, and block time, the reaction kinetics obtained from PRD simulations of hexadecane pyrolysis were compared to those obtained from direct MD simulations at a temperature of 2900 K—high enough so that thermal decomposition can be observed via direct MD simulations. The times required for the first decomposition reaction were recorded for a series of ten different initial conditions, using both direct MD and PRD with 61 processors ($M = 60$). Figure 2 shows the distribution function for the transition times of the ten initiation reactions from both direct MD and PRD simulations. Given an observation of N different event times t_1, \dots, t_N for a first-order process, the maximum likelihood (ML) estimator for the true rate constant is simply the inverse mean reaction time, $\tilde{k}_{\text{tot}} = \langle t_i \rangle^{-1}$. This ML rate constant was $\tilde{k}_{\text{tot}} = 1.24 \times 10^9 \text{ s}^{-1}$ from the direct MD simulations and $1.14 \times 10^9 \text{ s}^{-1}$ from the PRD simulations. A Kolmogorov-Smirnov test indicates that both empirical distribution functions are consistent with a first-order process with $k = 1.24 \times 10^9 \text{ s}^{-1}$, at the 90% confidence level. These results demonstrate that, at 2900 K where the direct dynamics simulation is feasible, PRD simulation does not perturb the kinetics of the thermal decomposition process. This is a good indication that the conformational space is still being sampled sufficiently within each replica. Additional details on the 2900 K simulations are available in Ref. 30. At lower temperatures, no comparison with direct MD is possible, because the decomposition does not take place in times that are easily accessible on a single processor. Fortunately, the efficiency of the conformational sampling will improve even further at lower temperatures, because the conformational

barriers are lower than those separating distinct chemical species. Consequently, we expect that the PRD simulations will continue to reproduce the correct reaction kinetics as the temperature is decreased.

We emphasize here that the validation of the PRD algorithm used here is a fairly general conclusion, and does not depend critically on the hydrocarbon model used. Although the AIREBO potential was chosen as the best available classical model for treating reactivity in hydrocarbons, it is still an approximate model (as are all classical potentials). Other potentials (including *ab initio* potential energy surfaces) will have small ($\lesssim 10$ kcal/mol) differences in barrier heights. These differences may have a large effect on the kinetics, but will not substantially affect the gap between conformational and covalent energy barriers. Thus, for any reasonable potential energy surface for hydrocarbons, the difference in rates for conformational and chemical reaction dynamics is large enough that the topology-based transition detection method can be safely used at temperatures below 3000 K.

B. Initiation

Table I shows the time and type of initiation reaction for a series of ten different initial conditions at five temperatures ranging from 2100 to 2500 K. The individual initiation times ranged from 0.04 to 789.76 ns. Note that the longest simulation would have required ≈ 26 months of continuous calculation on a single processor. By using PRD on 61 nodes of the computational “minigrad” at Clemson University, this simulation could be performed with a parallel efficiency of over 90%—far better than could be achieved on this 50-atom system by any atom-based parallel decomposition method.

The thermal decomposition of hydrocarbons has been extensively studied previously, and is known to involve a number of free radical species and radical chain reactions.^{2,3,34} In most simple reaction dynamics models, the mechanism for *n*-alkane pyrolysis is based on that proposed by Kossiakoff and Rice,⁶ and is assumed to take place through an initial homolytic scission of a C–C bond to produce two alkyl radicals, followed by a network of competing propagation reactions involving radical species. Initiation takes place via C–C bond dissociation because this bond is weaker than the C–H bonds (≈ 88 kcal/mol for a C–C dis-

sociation vs 100 kcal/mol for C–H).³ The actual initiation reaction is a composite reaction, with dissociation in varying proportions at symmetrically distinct C–C bonds (each with different Arrhenius parameters) at different temperatures. This mechanism is supported by various experimental results and the kinetics for the composite reaction are approximately first order at temperatures up to about 1000 K.^{1,8–10,35–37} Despite the use of the PRD algorithm, however, the simulation temperatures are still considerably higher than those commonly studied experimentally. At sufficiently high temperatures, initiation by C–H dissociation will become more prevalent. The rate of the C–H dissociations will be enhanced, relative to the C–C dissociations, by a factor of $\exp\{(\Delta E_a)/R[(1/T_1) - (1/T_2)]\}$ as the temperature increases from T_1 to T_2 . This increase is approximately a factor of 50 as the temperature is increased from 1000 to 2500 K, for example. The issue of whether C–H dissociations occur has only rarely been addressed experimentally,^{18,38} and has not been treated in previous kinetic models of heavy alkane pyrolysis, even for those studies performed at temperatures exceeding 1000 K.^{5,36}

When the data from each of the different temperatures is combined, the ratio of C–H to C–C bond dissociations is 41:9. Initiation via C–H bond dissociation is more frequent at these high temperatures, despite the fact that C–C bond dissociations have a lower activation barrier. This C–H:C–C dissociation ratio is even larger than the 34:15 ratio of C–H to C–C bonds, suggesting that the frequency factor must be larger for C–H dissociation. This is not expected, based on commonly accepted values for the frequency factors.³⁸ These values are based on experiments for much smaller hydrocarbons, and do not take into account the fact that the prefactor for C–C dissociations will decrease much more rapidly with increasing molecular size than will that of the C–H dissociations due to the higher probability of recoil-based recombinations when both product fragments are heavier than C_2H_5 . This dependence of the frequency factor on the size of the products is not taken into account in most kinetic models, and cannot be addressed by equilibrium kinetic theories. Because the AIREBO model is realistic in its prediction of C–H and C–C bond dissociation energies and vibrational frequencies, it is difficult to say whether the unexpectedly high contribution of C–H dissociations at high temperatures is side effect of the AIREBO model, or whether there is a larger-than-expected dependence of frequency factor on bond position. Additional dynamics simulations are needed to further examine this point.

Nearly 25% of the C–H dissociations occurred at terminal methyl groups (primary carbons), generating a primary radical. This is higher than the ~12% that would be expected at these temperatures, given the 6:28 ratio of primary to secondary hydrogens and the activation energy for primary C–H dissociation that is higher than that for secondary C–H dissociation by $\Delta E_a = 2.0$ kcal/mol, if the frequency factors are identical:

$$\frac{k_p}{k_p + k_s} = \frac{6e^{(-\Delta E_a)/kT}}{6e^{(-\Delta E_a)/kT} + 28} \approx 0.12. \quad (9)$$

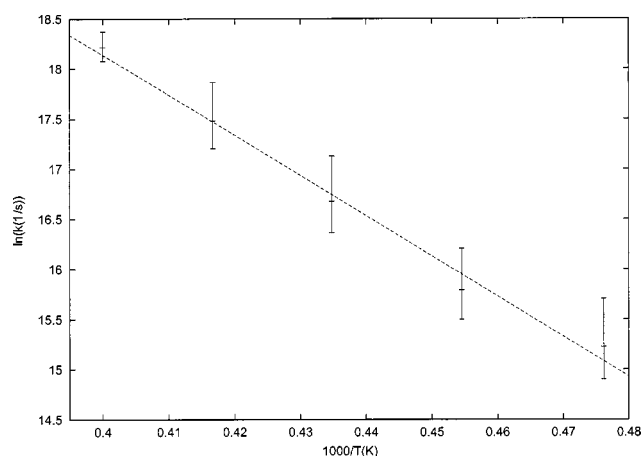


FIG. 3. Arrhenius plot of initiation rate constants in the temperature range of 2100–2500 K. Rate constants calculated from simulations are shown with error bars obtained from the 1σ interval on the mean reaction time, $[\langle(t + \sigma)^{-1}, \langle(t - \sigma)^{-1}\rangle]$, and a least squares fit (solid line).

It is reasonable to suppose that the frequency factor for C–H dissociation is larger on primary carbons, but the statistics are not sufficient to declare this difference significant.

None of the nine C–C dissociations occurred in the terminal C–C bond. While stronger than the internal C–C bonds by several kcal/mol, dissociations of the terminal bond should also be accessible at these temperatures, given the observation of C–H dissociations in addition to C–C dissociations, and primary C–H dissociations in addition to secondary C–H dissociations. Presumably they were not observed due to the limited sample size of only nine C–C dissociations.

Figure 3 shows the composite reaction rates for initiation as a function of temperature. The data fit well in this temperature range by the Arrhenius equation,

$$k_{\text{tot}} = A_0 \exp(-E_a/RT), \quad (10)$$

where A_0 is the frequency factor, E_a is the activation energy, R the universal gas constant, and T the absolute temperature. This results in an activation energy of $E_a = 79.7$ kcal/mol and a frequency factor of $\log(A_0/s^{-1}) = 14.8$. Experimental results for the initiation rate at lower temperatures also show Arrhenius behavior, with values of $\log A_0$ ranging from 14.3 to 19.6.^{3,8,9,39,40} The activation energy of 79.7 kcal/mol is also consistent with experimental and empirical model values, which range from 59 to 87 kcal/mol.^{3,8,9,39,40} Note that these Arrhenius parameters are composite parameters, and thus represent an average over all of the possible initiation modes. In the empirical model studies, the composite reactions are assumed to be solely C–C dissociations, whereas the current study includes C–H dissociations. Experimental studies, as well as the current dynamics simulations, consistently give Arrhenius activation energies lower than the barrier for the C–C dissociation reactions (88 kcal/mol from experiment; 92 kcal/mol using AIREBO). Values in the range of 75–80 kcal/mol for initiation are commonly accepted;² lower experimental activation energies for initiation are typically attributed to catalytic effects of the reactor walls,⁹ an effect that is absent in the current simulations.

TABLE II. Arrhenius parameters for the composite initiation reaction in the thermal decomposition of *n*-hexadecane.

Temperature (K)	$\log(A_0/s^{-1})$	E_a (kcal/mol)	Initiation modes	Method	Reference
623–793	18	80	CCD	Experiment	40
873–1023	14.3	59	CCD	Empirical model	8
652–723	14.8 ^a	67.0	CCD	Empirical model	9
n/a	18–19 ^a	88.0–RT	CCD	Heuristic	3
572–973	19.1–19.3	87.0	CCD	Empirical model	39
2100–2500	14.8	79.7	CHD(0.75):CCD(0.25)	PRD	This work

^aFrequency factors for single bond dissociations have been multiplied by the total number of bonds with equivalent energy (13 or 15 for C₁₆, depending on the model).

Arrhenius parameters from several studies at different temperatures are compared in Table II. While the frequency factors obtained here at over 2000 K are comparable to some of the literature values (at much lower temperatures), they are somewhat lower than expected; both the frequency factor and the activation energy should increase at elevated temperatures as additional reaction modes (such as C–H dissociation) begin to contribute. Our reaction rate at 2500 K of $6.8 \times 10^7 \text{ s}^{-1}$ is slower than the values of $1.4 \times 10^9 \text{ s}^{-1}$ through $1.1 \times 10^{12} \text{ s}^{-1}$ obtained by extrapolating the experimental results to 2500 K. While agreement is not to be expected after a 1500 K extrapolation, the fact that the current rate is lower than predicted indicates that the current model may overpredict the barriers or underestimate the frequency factors for some reaction channels. However, we also note that our data can be fit equally well with temperature-dependent prefactors,^{41,42} making any temperature extrapolation quite circumspect. Although the high temperatures used here prevent the validation of the AIREBO model directly against experiment, this model has proved successful in a range of other systems involving C–C and C–H bond dissociation. A detailed comparison of AIREBO reaction barriers with *ab initio* calculations is currently underway that should help to enable closer comparison with experiment.

C. Propagation

It is well understood that in pyrolysis, the chemistry subsequent to the initiation reaction takes place via radical chain reactions.^{2,3,34} The basic reactions in the chain have been well understood for half a century,^{6,7} and kinetic models exist which can predict approximate product distributions for the pyrolysis of linear alkanes. However, empirically adjusted model parameters often disagree markedly with known kinetic parameters, indicating that not all of the steps in the reaction network are fully understood at present. In addition, a thorough understanding of the kinetics and mechanisms of the underlying reactions will be required if we hope to make good predictions for cases that are not as well understood as simple alkanes.

A number of different kinetic models have been used in attempts to reproduce experimental results, including product ratios.^{6,8–11,13,15,34–37,43} These range from analytical theory to very coarse-grained models that lump many different reaction products into a small number of classes, to complex systems of hundreds of coupled differential equations. Direct comparison of the current results with experiment and with

the results of these models is not possible, for a number of reasons. The most important of these is that the current studies were performed with isolated molecules. No attempt was made to model collisions between gas-phase species. Consequently, important mechanistic steps such as hydrogen abstraction (intermolecular hydrogen transfer) and chain termination could not be observed. These reactions, especially hydrogen abstraction, can have a dramatic effect on the ultimate product distribution and its pressure dependence.^{2,6,7}

Although the simulations were performed without any intermolecular collisions, the rate of thermal activation in the simulations corresponds to the high-pressure limit. This is because the Langevin thermostat employed to control the temperature in these simulations used a friction value of $\zeta = 0.007 \text{ fs}^{-1}$. In a system with hard-sphere collisions, equivalent thermalization at a collision frequency of $\zeta \sim 0.007 \text{ fs}^{-1}$ would occur at an ideal gas pressure of⁴⁴ $P = (N/V)kT = (\zeta/\langle v^2 \rangle^{1/2} \pi d^2)kT$. Assuming a hard sphere diameter of $d \sim 1 \text{ nm}$ and a root mean square velocity of $\langle v^2 \rangle^{1/2} = 700 \text{ m s}^{-1}$ at $T = 2500 \text{ K}$, this corresponds to a pressure of ~ 1000 bars. In other words, the energy transfer between a molecule or radical and the thermal heat bath occurs at a rate corresponding to high-pressure or liquid-state conditions, with energy transfer modeled via the Langevin thermostat rather than by explicit collisions. Additional evidence that the results obtained here correspond to the high-pressure limit comes from the observation that, in initial investigations, varying the thermostat time constant between 30 and 100 fs had no effect on the rate.

We have neither further explored the pressure dependence of the rate constants nor have we attempted to evaluate the energy dependence of the microcanonical rate constant that could be used for Rice–Ramsperger–Kassel–Marcus (RRKM) calculations of the rate. The simulations were all in the canonical ensemble, and thus provide an average over microcanonical rates. We emphasize once more that the principal aim was to perform a dynamics simulation of thermal decomposition without imposing any biases due to an assumed reaction network or set of kinetic parameters. Although additional studies with more accurate models and treatment of intermolecular effects will be needed before kinetic data can be applied directly to improved empirical models, successful validation of the algorithm provides the groundwork for such future studies.

To study the unimolecular radical propagation reactions, we performed additional PRD simulations of ten consecutive

TABLE III. Ten consecutive transitions, along with the initial and final reaction times, for the first of three initial configurations. A C–C dissociation between atoms i and j in the carbon backbone is indicated by the notation CCD(i : j); the notation CHD(i) indicates a hydrogen dissociated from carbon i ; HTR(i : j) indicates a hydrogen transfer from carbon i to carbon j ; intramolecular cyclization via bond formation between carbon atoms i and j is indicated by NMRF(i : j) to indicate the formation of an N -membered ring; the notation NMRD(i : j) indicates that an N -membered ring has broken at the bond between carbons i and j (a special case of C–C dissociation) without resulting in dissociation of the molecule.

Temperature (K)	1	2	3	4	5	6	7	8	9	10	t_1 (ns)	t_{10} (ns)
2500	CHD (1)	HTR (2:1)	HTR (3:2)	HTR (4:2)	HTR (5:4)	HTR (6:5)	HTR (5:6)	HTR (6:5)	HTR (5:6)	HTR ^a (6:5)	8.74	14.99
2400	CHD (7)	HTR (8:7)	CHD (8)	CHD (15)	CHD (16)	CHD (1)	HTR (2:1)	HTR ^b (1:2)	3MRD ^b (1:3)	3MRD (1:3)	58.86	67.35
2300	CHD (9)	HTR (8:9)	HTR (7:8)	HTR (6:7)	HTR (7:6)	HTR (6:7)	HTR (7:6)	CHD (6)	CHD (5)	CHD (8)	16.79	24.55
2200	CHD (16)	HTR (15:16)	CHD (16)	CHD (13)	3MRF ^c (13:15)	3MRF ^c (13:15)	3MRF ^c (13:15)	3MRF ^c (13:15)	3MRF ^c (13:15)	3MRF (13:15)	39.69	270.89
2100	CHD (9)	HTR (10:9)	HTR (9:10)	HTR (10:9)	CHD (11)	CHD (6)	HTR (5:6)	HTR (4:5)	HTR (5:4)	HTR (6:5)	37.18	105.32

^aHTR(5:6) occurred simultaneously.

^b3MRF(1:3) occurred during the subsequent correlation period.

^c3MRD(13:15) occurred during the subsequent correlation period.

reactions (beginning with the initiation reaction) for each of three independent initial configurations of n -hexadecane in the same temperature range of 2100–2500 K. A total of over 1.35 μ s of dynamics was run on these systems, using PRD on 61 processors. Parallel replica dynamics is clearly invaluable in extending the range of simulation temperatures and times. Even in cases such as this where the independent simulations could have been parallelized trivially across as many as 15 different processors, the longest simulations, requiring hundreds of nanoseconds would have taken many months on a single processor; PRD is useful not only for increasing the number of processors onto which the problem can be parallelized, but also in providing a sort of load balancing.

A total of 150 independent (noncorrelated) reactions were thus observed: 15 initiation and 135 propagation reactions. From these, we identified five distinct reaction mechanisms: (1) carbon-carbon dissociation (CCD); (2) carbon-hydrogen dissociation (CHD); (3) intramolecular hydrogen transfer or hydrogen shift reactions (HTR); (4) three membered ring formation (3MRF); (5) three membered ring dis-

sociation (3MRD). The details of all 150 independent reactions are presented in Tables III–V, along with the first and tenth reaction times. (Note that occasionally, during the 40 ps correlation time following a reaction, a subsequent reaction would occur. Such reactions are conservatively assumed to be correlated with the previous reaction and are not counted as independent events.)

The most common chain reaction was an internal hydrogen transfer reaction, which occurred 75 times among the 135 independent propagation reactions (56%). The fast rate of this isomerization reaction confirms that the radical site is highly mobile, and at low pressures it is safe to assume an equilibrium distribution of isomeric radical species. Isomerization also occurred via three-membered ring formation (10 reactions; 7%) and dissociation of three-membered rings (11 reactions; 8%).⁴⁵ Ignoring the 15 initiation reactions, dissociation took place via C–H bond cleavage in 33 instances (24%) and via C–C bond cleavage in 6 instances (4%), again showing the prevalence of C–H dissociation at high temperatures with this model. The statistics on any one of these reaction modes at a particular temperature are not extensive,

TABLE IV. Ten consecutive transitions, along with the initial and final reaction times, for the second of three initial configurations. Description of reactions as in Table III.

Temperature (K)	1	2	3	4	5	6	7	8	9	10	t_1 (ns)	t_{10} (ns)
2500	CHD ^a (9)	CHD (11)	CHD (4)	CHD (3)	CCD (5:6)	3MRF ^b (3:5)	CHD (4)	HTR (7:6)	CHD (7)	CCD (13:14)	6.95	39.82
2400	CHD (14)	HTR (13:14)	HTR (14:13)	HTR (15:14)	HTR (14:15)	HTR (16:14)	HTR (15:16)	HTR (14:15)	CHD ^c (1)	CHD (15)	4.21	14.08
2300	CHD (9)	HTR (10:9)	HTR (9:10)	HTR (8:9)	HTR (9:8)	HTR (10:9)	HTR (11:10)	HTR (12:11)	HTR (11:12)	HTR (12:11)	0.04	20.61
2200	CHD (6)	HTR (5:6)	HTR (6:5)	HTR (7:6)	HTR (6:7)	HTR (7:6)	HTR (6:7)	CCD (4:5)	HTR (3:4)	HTR (2:3)	21.76	45.38
2100	CCD (12:13)	HTR (11:12)	HTR (14:13)	HTR (12:11)	HTR (11:12)	CHD (13)	HTR (10:11)	HTR (9:10)	HTR (8:9)	HTR (9:8)	236.94	299.06

^aHTR(10:9) occurred during the subsequent correlation period.

^b3MRD(3:5) occurred during the subsequent correlation period.

^cHTR(2:1) occurred during the subsequent correlation period.

TABLE V. Ten consecutive transitions, along with the initial and final reaction times, for the third of three initial configurations. Description of reactions as in Table III.

Temperature (K)	1	2	3	4	5	6	7	8	9	10	t_1 (ns)	t_{10} (ns)
2500	CHD (4)	CCD (5:6)	CHD (7)	HTR (6:7)	HTR (8:6)	CHD ^a (5)	3MRD ^b (6:7)	3MRD ^b (6:7)	3MRD ^b (6:7)	3MRD (6:8)	4.32	18.04
2400	CHD (14)	CHD (15)	CHD (16)	3MRF ^c (14:16)	CHD (13)	CHD (12)	CHD (11)	CHD (15)	HTR (14:15)	3MRF (12:14)	42.82	138.99
2300	CHD (14)	HTR (13:14)	HTR (12:13)	HTR (13:12)	CCD (12:13)	HTR (11:12)	HTR (10:11)	HTR (9:10)	CHD (8)	CHD (14)	93.79	109.72
2200	CHD (8)	HTR (9:8)	CHD (9)	CHD (16)	HTR (15:16)	HTR (16:15)	HTR (15:16)	CHD (16)	CHD (6)	3MRF (6:8)	19.56	93.05
2100	CHD (12)	HTR (11:12)	CCD (6:7)	HTR (8:7)	HTR ^d (10:11)	3MRD ^d (8:10)	3MRD ^e (8:9)	3MRD ^e (8:9)	3MRD ^f (8:10)	3MRD (8:10)	104.03	124.34

^a3MRF(6:8) occurred during the subsequent correlation period.

^b3MRF(6:7) occurred during the subsequent correlation period.

^c3MRD(14:16) occurred during the subsequent correlation period.

^d3MRF(8:10) occurred during the subsequent correlation period.

^e3MRF(8:9) occurred during the subsequent correlation period.

^f3MRF(8:10) occurred during the subsequent correlation period.

so we do not provide individual reaction rates or Arrhenius parameters.

Hydrogen transfer is by far the fastest of the unimolecular propagation reactions, representing over half of the independent reactions observed. Kinetic models, such as those based on the theory of Kossiakoff and Rice,⁶ frequently assume that internal hydrogen transfer occurs between (1,5) carbons in order to minimize strain energy in the cyclic transition state (which is a six-membered ring in this case). In contrast, nearly all the hydrogen transfers in our simulations occurred via (1,2) hydrogen transfer, via a triangular transition state. Hydrogen transfer to distant sites did occur, but generally by diffusion of the radical site via repeated one-site hops. In selected cases, hydrogen transfer occurred via a (1,3) two-site hop (e.g., reaction 6 at 2400 K in Table IV and reaction 5 at 2500 K in Table V), and via concerted, nearly simultaneous exchange of two vicinal hydrogens (reaction 10 at 2500 K in Table III). The mechanistic details of intramolecular hydrogen transfer and their influence on hydrocarbon pyrolysis products have been debated frequently in the past.² Hydrogen transfer via (1,4) shift is known experimentally to occur,^{46–48} and is fast enough at low temperatures that it is often required in kinetic models in order to reproduce experimental product distributions.^{40,43,49,50} Shorter-distance hydrogen transfers [including (1,2) transfers between vicinal carbons] are also known to occur in selected instances, albeit with larger barriers than the (1,4) and (1,5) transfers.^{20,51} For large molecules, the presence of shorter-distance hydrogen transfers is perhaps irrelevant, as a full distribution of primary and secondary radicals can be obtained for all species larger than the pentyl radical using no hydrogen transfers shorter than (1,4). But shorter hops, if they occur, would affect the distribution of products obtained from smaller radical species generated during the decomposition process.

It is generally believed that hydrogen transfers shorter than (1,4) do not occur at experimental temperatures,³ although the reactions themselves are not observed directly, and the arguments are typically made from indirect evidence of the product distributions. The primary evidence against (1,2) hydrogen transfers comes from pyrolysis studies of deuterated butane, in which decomposition products result-

ing from pathways involving (1,2) hydrogen transfer are not observed.⁵² However, this result merely illustrates that pathways involving (1,2) hydrogen transfer are not competitive with those involving β -scission [and possibly including (1,3) hydrogen transfer] at temperatures below 800 K. Although we do not present detailed reaction rates for hydrogen transfer due to the limited sample sizes, it is clear from the simulation results that the higher prefactor associated with short-range hydrogen transfer more than outweighs the additional strain energy at the barrier at these elevated temperatures in the AIREBO model used here. Given the difference between experimental and simulation temperature scales, it is important to validate the AIREBO model directly against more accurate *ab initio* calculations. Detailed analysis of the reaction pathways, transition states, and activation energies observed here will allow more conclusive statements about whether these reactions are expected to be important at experimentally relevant temperatures. Such studies are currently underway, both with classical and *ab initio* potential energy surfaces.

Isomerization of the carbon backbone occurred in the PRD simulations via the formation and dissociation of cyclic structures. Cyclization reactions are typically ignored entirely in kinetic models. In the simulations, ring formation occurred exclusively in the form of transient, highly strained cyclopropyl rings. As with the hydrogen transfer reaction, the higher prefactor for the formation of small cyclic structures overcomes the higher strain energy at these elevated temperatures. Of the 156 reactions observed (including 21 correlated events and excluding the 15 initiation reactions), 21 were cyclopropyl ring-closings and 18 were ring-opening reactions. Although the cyclopropyl species are stable, they are very short lived at these temperatures, nearly always decomposing to the preceding structure within tens of picoseconds (often within the 40 ps correlation time). On two occasions, however (reactions 7–9 at 2500 K and reactions 7–8 at 2100 K in Table V), the cyclopropyl species survived long enough for the energy to dissipate from the incipient bond, dissociating instead into a branched compound as illustrated in Fig. 4. To the extent that the three-membered ring structures are transient intramolecular “complexes,” it is unim-

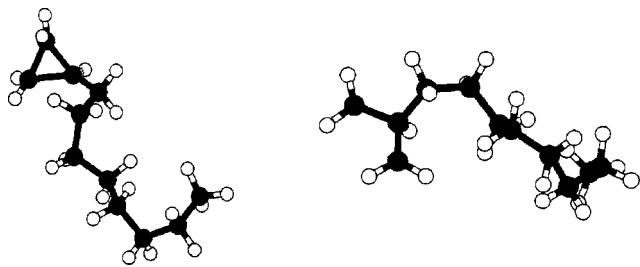


FIG. 4. Isomerization of $C_{11}H_{22}$, an intermediate decomposition product, from a cyclopropyl structure (octylcyclopropane, left panel) to a branched diradical (2-nonylpropane-1,3-diyl, right panel). Black atoms are carbons and white atoms are hydrogens. This reaction occurred as the seventh transition at 2500 K in Table V.

portant to include them in a coarse-grained kinetic model. However, given that they occasionally result in isomerization reactions, inclusion of these strained ring structures could have some effect in the predicted (small) fraction of branched products. Once again, it is uncertain to what degree these conclusions will hold at lower temperatures, and to what degree their presence is an artifact of the potential model. More detailed investigation of these structures and their energetics is underway.

As with the more comprehensive results on initiation reactions presented in Table I, the majority of initiation reactions (93%) occurred via C–H dissociation. C–H dissociation was also more prevalent after initiation, numbering 34 of the 156 post-initiation reactions, vs six C–C dissociations. Half of the observed C–C dissociations were β -scission reactions in which the C–C bond β to a radical site is cleaved. This is one of the most important chain propagation steps in the Kossiakoff-Rice mechanism, so it is not surprising that it also features prominently in the simulations, even at high temperature. The three instances where it was observed were in reaction 8 at 2200 K in Table IV, reaction 2 at 2500 K in Table V, and reaction 5 at 2300 K in Table V.

Detailed analysis of Tables III through V reveals a number of other interesting mechanistic observations. For example, generation of a primary radical (via either C–C or primary C–H dissociation) was usually followed shortly by hydrogen transfer reactions resulting in a lower-energy secondary radical. And C–H dissociations frequently occurred adjacent to existing radical or π -bonding sites, leading to conjugated π systems. A conjugated triene was formed in this manner at 2400 K in Table IV.

IV. CONCLUSIONS

Parallel replica dynamics has been applied to study a system with a heterogeneous distribution of reaction barriers. By detecting transitions using molecular connectivity, rather than absolute geometry of the configuration, we have been able to apply the PRD algorithm to the pyrolysis of hexadecane, in which there are a range of large (reactive) and small (conformational) energy barriers. A number of other processes including activated processes in liquids, polymers, and biomolecules may benefit from the same approach.

The PRD results for hexadecane agree with those of direct MD simulation at a temperature of 2900 K, confirming

that the PRD algorithm can be used with confidence for this system, as well as other systems with comparably large ratios of conformational to chemical reaction rates. Use of the PRD algorithm with connectivity-based transition detection allowed parallel simulation with more processors than atoms in the system, and enabled simulations of hydrocarbon pyrolysis at temperatures of 2100–2500 K, some 1000 K lower than had been previously attempted with direct dynamics simulations. A total of over 5 μ s of dynamics was performed on this system, a feat which would not have been possible with alternative parallelization methods. Indeed, the parallel efficiency of over 90% achieved in this study on 61 processors requires an implementation that is over 99.8% parallel (according to Amdahl's Law), even if the communication costs are assumed to be zero. Performance at this level would clearly be impossible for systems of this size with traditional parallelization methods.

Several aspects of the kinetics were in agreement with experimental results at lower temperatures. The dissociation was found to be first order, and to have an Arrhenius-type temperature dependence. The Arrhenius parameters were in good general agreement with those obtained by fitting empirical models to experimental results, although the extrapolated rates were lower than the empirical values. After initiation, the unimolecular propagation steps that could be observed in these simulations involved fast mobility of the radical site via hydrogen-transfer reactions, and decomposition due to β -scission (and other scission) reactions.

Other details of the observed mechanism are more unusual, and do not occur or are not included in kinetic models at lower temperatures. These include the observation that dissociation occurs primarily via C–H bond cleavage at these temperatures, that hydrogen transfer occurs predominantly between vicinal carbons, and that the carbon backbone isomerizes generating branched structures via transient cyclic structures.

We note that the accuracy of the results obtained here depend on the accuracy of both the algorithm and the potential used. The algorithm has been verified for this system, by comparing reaction time distributions for direct MD and PRD. While the AIREBO potential has proved successful in other reactive hydrocarbon systems, it has not been specifically validated for the case of hydrocarbon pyrolysis. Such validation is currently underway through comparison with *ab initio* calculations. These studies will enable more definitive statements about whether the unexpected reactions are a consequence of the elevated temperature of the simulations, or the hydrocarbon potential. Although the high-barrier reactions are not expected to play major roles in pyrolysis mechanisms below 1000 K, the higher temperatures being used in modern pyrolysis experiments necessitate the careful treatment of high-energy reaction channels in kinetic models.¹⁸

Independent of the quality of the potential, an important result from this study is that the PRD technique, with the transition detection scheme used here, can be used with confidence for simulations of hydrocarbon pyrolysis with any realistic potential. A comprehensive program based on long-time exploratory simulations with approximate potentials,

followed by accurate calculations with quantum mechanical methods, can be expected to provide improvements to large-scale kinetic models. In addition, the method developed here can also be used for a wide range of other rare events in conformationally complex systems.

The combination of the PRD algorithm and the AIREBO reactive potential in this study has enabled simulations of hydrocarbon pyrolysis at temperatures as low as 2100 K, for aggregate times of over 5 μ s. We expect that by using massively parallel PRD, or by combining PRD with complementary accelerated dynamics techniques such as temperature-accelerated dynamics,⁵³ accurate simulations of fuel oil hydrocarbon pyrolysis might be possible at temperatures approaching 1000 K, particularly for the propagation reactions. One significant advantage of this simulation technique is that the reaction modes and mechanisms have not been predetermined, as in kinetic models. The transitions are discovered purely as a result of the dynamics exploring the potential energy surface. The power of this method is evident in the fact that several unexpected mechanisms were uncovered. Whether these lead to improvements in kinetic models, or to improvements in the classical potentials, we expect that they will contribute to a more complete understanding the dynamics of this complex process.

ACKNOWLEDGMENTS

Dan Stanzione is thanked for his assistance with the Clemson Computational Minigrad Beowulf cluster facility. Financial support by the Department of Energy Grant No. (DE-FG02-01ER45889), the National Science Foundation Grant No. (CHE-0239448), and the donors of the Petroleum Research Fund Grant No. (35637-G6) is gratefully acknowledged. Work at LANL was supported by the U.S. Department of Energy, Office of Science, Office of Basic Energy Sciences, under DOE Contract No. W-7405-ENG-36; and through a CRADA with Motorola, Inc.

¹P. Ungerer, *Adv. Org. Geochem.* **16**, 1 (1990).

²I. Safarik and O. P. Strausz, *Res. Chem. Intermed.* **22**, 275 (1996).

³M. L. Poutsma, *J. Anal. Appl. Pyrolysis* **54**, 5 (2000).

⁴D. W. Waples, *Org. Geochem.* **31**, 553 (2000).

⁵J. A. Fairburn, L. A. Behie, and W. Y. Svrcek, *Fuel* **69**, 1537 (1990).

⁶A. Kossiakoff and F. O. Rice, *J. Am. Chem. Soc.* **65**, 590 (1943).

⁷B. M. Fabuss, J. O. Smith, and G. N. Satterfield, *Adv. Petr. Chem. Refin.* **3**, 156 (1964).

⁸D. Depeyre and C. Flicoteaux, *Ind. Eng. Chem. Res.* **30**, 1116 (1991).

⁹F. Khorasheh and M. R. Gray, *Ind. Eng. Chem. Res.* **32**, 1853 (1993).

¹⁰K. J. Jackson, A. K. Burnham, R. L. Braun, and K. G. Knauss, *Org. Geochem.* **23**, 941 (1995).

¹¹M. Vandembroucke, F. Behar, and J. L. Rudkiewicz, *Org. Geochem.* **30**, 1105 (1999).

¹²G. R. Gavalas, *Chem. Eng. Sci.* **21**, 133 (1966).

¹³D. L. Allara and D. Edelson, *Int. J. Chem. Kinet.* **7**, 479 (1975).

¹⁴D. S. Aribike and A. A. Susu, *Thermochim. Acta* **127**, 259 (1988).

¹⁵P. Mousquès, J. L. Dirion, and D. Grouset, *J. Anal. Appl. Pyrolysis* **58–59**, 733 (2001).

¹⁶Y. T. Xiao, J. M. Longo, G. B. Hieshima, and R. J. Hill, *Ind. Eng. Chem. Res.* **36**, 4033 (1997).

¹⁷L. C. Jitariu, H. Wang, I. H. Hillier, and M. J. Pilling, *Phys. Chem. Chem. Phys.* **3**, 2459 (2001).

¹⁸N. Yamauchi, A. Miyoshi, K. Kosaka, M. Koshi, and H. Matsui, *J. Phys. Chem. A* **103**, 2723 (1999).

¹⁹E. Goldstein, M. Haught, and Y. Tang, *J. Comput. Chem.* **19**, 154 (1998).

²⁰B. Viskolcz, G. Lendvay, and L. Seres, *J. Phys. Chem. A* **101**, 7119 (1997).

²¹D. W. Brenner, *Phys. Rev. B* **42**, 9458 (1990).

²²D. W. Brenner, O. A. Shenderova, and J. A. Harrison, *J. Phys.: Condens. Matter* **14**, 783 (2002).

²³S. J. Stuart, A. B. Tutein, and J. A. Harrison, *J. Chem. Phys.* **112**, 6472 (2000).

²⁴S. J. Stuart, B. M. Dickson, D. W. Noid, and B. J. Sumpter, *Mater. Res. Soc. Symp. Proc.* **651**, T7.15.1 (2001).

²⁵M. R. Nyden and D. W. Noid, *J. Phys. Chem.* **95**, 940 (1991).

²⁶A. F. Voter, *Phys. Rev. B* **57**, R13985 (1998).

²⁷A. F. Voter, F. Montalenti, and T. C. Germann, *Annu. Rev. Mater. Sci.* **32**, 321 (2002).

²⁸M. R. Shirts and V. S. Pande, *Phys. Rev. B* **86**, 4983 (2001).

²⁹M. Shirts and V. S. Pande, *Science* **290**, 1903 (2000).

³⁰O. Kum, B. M. Dickson, S. J. Stuart, B. P. Uberuaga, and A. F. Voter, in *Parallel and Distributed Computing Systems*, edited by S. G. Akl and T. Gonzalex (ACTA Press Anaheim, 2002), pp. 507–513.

³¹A. F. Voter and J. D. Doll, *J. Chem. Phys.* **82**, 80 (1985).

³²V. S. Pande and D. S. Rokhsar, *Proc. Natl. Acad. Sci. U.S.A.* **96**, 1273 (1999).

³³J. Tersoff, *Phys. Rev. B* **37**, 6991 (1988).

³⁴P. E. Savage, *J. Anal. Appl. Pyrolysis* **54**, 109 (2000).

³⁵B. Blouri, F. Hamdan, and D. Herculat, *Ind. Eng. Chem. Process Des. Dev.* **24**, 30 (1985).

³⁶D. Depeyre, C. Flicoteaux, and C. Chardaire, *Ind. Eng. Chem. Process Des. Dev.* **24**, 1251 (1985).

³⁷P. Zhou, O. L. Hollis, and B. L. Crynes, *Ind. Eng. Chem. Res.* **26**, 846 (1987).

³⁸A. M. Dean, *J. Phys. Chem.* **89**, 4600 (1985).

³⁹M. Watanabe, T. Adschiri, and K. Arai, *Ind. Eng. Chem. Res.* **40**, 2027 (2001).

⁴⁰F. Doue and G. Guiochon, *J. Chim. Phys. Phys.-Chim. Biol.* **65**, 395 (1968).

⁴¹A. Redondo, Y. Zeiri, J. J. Low, and W. A. Goddard III, *J. Chem. Phys.* **79**, 6410 (1983).

⁴²R. Font and A. N. Garcia, *J. Anal. Appl. Pyrolysis* **35**, 249 (1995).

⁴³F. Doue and G. Guiochon, *J. Phys. Chem.* **73**, 2804 (1969).

⁴⁴J. I. Steinfeld, J. S. Francisco, and W. L. Hase, *Chemical Kinetics and Dynamics*, 2nd ed. (Prentice Hall, Upper Saddle River, NJ, 1999).

⁴⁵Including the correlated reactions, there were 21 3MRF and 18 3MRD.

⁴⁶R. M. Marshall, *Int. J. Chem. Kinet.* **22**, 923 (1990).

⁴⁷A. S. Gordon and J. R. McNesby, *J. Chem. Phys.* **31**, 853 (1959).

⁴⁸L. Endrenyi and D. J. L. Roy, *J. Phys. Chem.* **70**, 4081 (1966).

⁴⁹K. H. Ebert, H. J. Ederer, and G. Isbarn, *Int. J. Chem. Kinet.* **15**, 475 (1983).

⁵⁰F. Billaud and E. Freund, *Ind. Eng. Chem. Fundam.* **25**, 433 (1986).

⁵¹A. S. Gordon, D. C. Tardy, and R. Ireton, *J. Phys. Chem.* **80**, 1400 (1976).

⁵²J. R. McNesby, C. M. Drew, and A. S. Gordon, *J. Chem. Phys.* **24**, 1260 (1956).

⁵³M. R. Sorenson and A. F. Voter, *J. Chem. Phys.* **112**, 9599 (2000).